Scanning Hall Probe Microscopy of Vortex Matter

Simon J. Bending

Department of Physics, University of Bath, Claverton Down, Bath BA2 7AY, UK

Elsevier use only: Received date here; revised date here; accepted date here

Abstract

Scanning Hall probe microscopy (SHPM) is a novel scanned probe magnetic imaging technique whereby the stray fields at the surface of a sample are mapped with a sub-micron semiconductor heterostructure Hall probe. In addition an integrated scanning tunnelling microscope (STM) or atomic force microscope (AFM) tip allows the simultaneous measurement of the sample topography, which can then be correlated with magnetic images. SHPM has several advantages over alternative methods; it is almost completely *non-invasive*, can be used over a very wide range of temperatures (0.3-300K) and magnetic fields (0-7T) and yields *quantitative* maps of the z-component of magnetic induction. The approach is particularly well suited to low temperature imaging of vortices in type II superconductors with very high signal:noise ratios and relatively high spatial resolution (>100nm). This paper will introduce the design principles of SHPM including the choice of semiconductor heterostructure for different measurement conditions as well as surface tracking and scanning mechanisms. The full potential of the technique will be illustrated with results of vortex imaging studies of three distinct superconducting systems; (ii) vortex chains in the "crossing lattices" regime of highly anisotropic cuprate superconductors, (ii) vortex-antivortex pairs spontaneously nucleated in ferromagnetic-superconductor hybrid structures and (iii) vortices in the exotic p-wave superconductor Sr_2RuO_4 at milliKelvin temperatures.

Scanning Probe Microscopy; Magnetic Imaging; Vortices; Type II Superconductors
07.79.-v; 74.25.Qt; 75.60.Ch; 75.47.-m

1. Introduction

High resolution magnetic imaging has long been a key diagnostic tool in a number of critical technological areas, e.g. magnetic data storage, spintronics and superconductivity. The technique of choice in the data storage industry is currently magnetic force microscopy (MFM) due, in part, to its easy implementation and good spatial resolution at room temperature. MFM, however, has a number of short-comings as well as being challenging to implement at low temperatures. The magnetic tip can be highly invasive, and quantitative image interpretation is difficult, requiring a precise model for the magnetisation state of the tip which is rarely available. To address these issues a complementary scanning probe technique based on nanoscale Hall-effect sensors has evolved over the last decade, enabled by recent breakthroughs in semiconductor heterostructure growth. This approach is almost completely non-invasive, can be used over a wide range of temperatures (0.3–300 K) and magnetic fields (0–7 T) and is particularly valuable when quantitative maps of magnetic induction are required with very high signal:noise ratios.

2. Principle of operation, experimental methods

The use of Hall effect sensors to image superconducting and ferromagnetic materials can be traced back well over 40 years and thin evaporated films of Bi [1,2] or InSb [3,4] have typically been employed in this role. Despite the fact

that most of these early studies used micrometer-based scanning stages with limited precision and reproducibility to capture data, spatial resolution as high as 4 μm with minimum detectable fields of ~0.01 mT were already achieved in ref. [2]. The invention of high mobility modulation-doped semiconductor heterostructures [5] and the development of piezoelectric nanoscale positioning systems [6] in the late seventies and early eighties have revolutionised the field in the last two decades.

2.1. Sensor Materials Issues

Developing scanning Hall probe systems for different operation conditions is primarily a Hall probe material optimisation problem. The signal:noise ratio (*SNR*), which is limited by Johnson noise at frequencies above the *1/f* noise corner, is a key figure-of-merit which determines the minimum detectable field of the sensor:

$$SNR = \frac{I_{\max} R_H B}{\sqrt{4kTR_V \Delta f}} \propto \sqrt{\mu / n_{2d}} \times I_{\max} \qquad (1)$$

where R_H is the Hall coefficient, R_V is the output resistance at the voltage contacts, Δf is the measurement bandwidth and μ and n_{2d} are the two-dimensional carrier mobility and concentration respectively. I_{max} is a maximum empirical operation current which, at high temperatures, is generally limited by the saturation drift velocity [7]. At low temperatures electron transport in the sensor can be quasiballistic and I_{max} is associated with a rapid increase in *1/f* noise which can have several different origins.

Most modern scanning Hall probe systems employ epitaxial GaAs/AlGaAs heterostructure Hall probes in which a 2D electron gas (2DEG) is trapped in a V-shaped potential well at the interface between slabs of n-AlGaAs and GaAs, separated from the ionised donors by an undoped AlGaAs spacer layer [8,9]. On cooling from 300K to 4.2K R_V in such sensors typically decreases by a factor of 30 while I_{max} increases by a factor of 10, resulting in an overall decrease in the noise-equivalent field (NEF) of two orders of magnitude to around 70 nT/Hz$^{0.5}$ above the *1/f* corner. Remarkably the Hall coefficient only changes by about 25% over the same temperature range, yielding a rather stable sensor sensitivity.

Unfortunately the advantages of high electron mobilities in GaAs/AlGaAs heterostructures at low temperature are largely lost at 300K due to a substantial reduction in carrier mobility arising from the additional phonon scattering. In this high temperature regime a better approach is often to use narrow gap semiconductors (e.g. InSb and InAs) which have very small effective electron masses (m_e*(InSb)=0.014m_0, m_e*(InAs)=0.023m_0, m_e*(GaAs)=0.067m_0) and intrinsically low scattering rates. Sensors can be patterned from narrow gap epitaxial quantum well structures (e.g. GaSb/InAs/GaSb) or polycrystalline thin films (e.g. InSb). InSb appears particularly promising with 300K electron mobilities as high as 50,000 cm^2/Vs being reported. Unfortunately the epitaxial growth of InSb is challenging, and very thin polycrystalline films, which would be required to pattern nanoscale sensors, have poor quality. Recent work, however, on δ-doped InSb quantum well structures [10] looks very encouraging for future imaging applications.

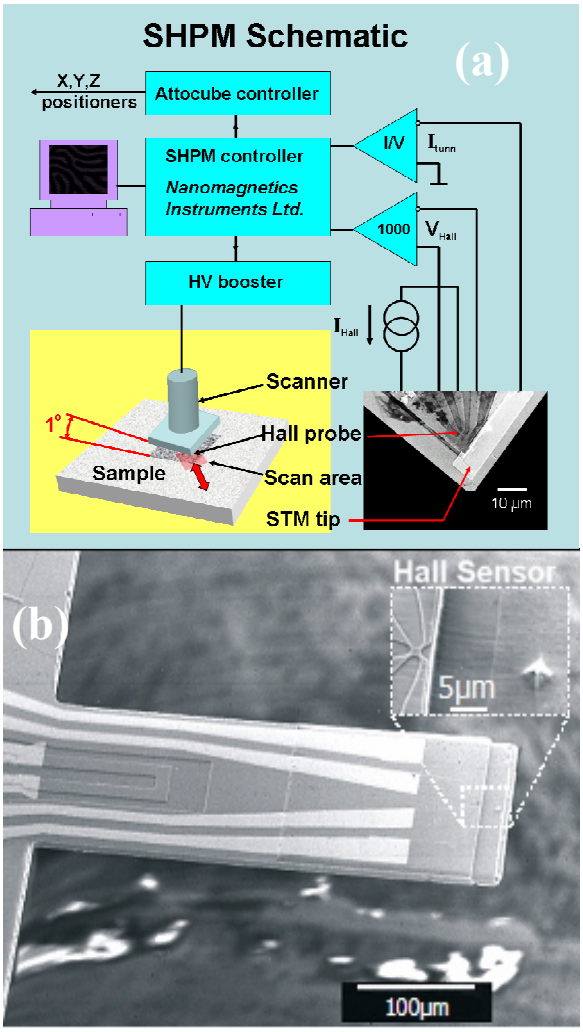

Fig. 1 (colour online) (a) Schematic diagram of a typical SHPM system with STM-tracking. (b) Optical image of an AFM-tracking sensor with an integrated piezoresistor for deflection detection.

Materials with the highest low temperature figures-of-merit do not often make the best choice for fabricating sensors with the highest spatial resolution. This is because sidewall depletion of narrow 'wires' typically result in the *electronic* width being much narrower than the *geometrical* width (generally by ~200nm), an effect that is very difficult to account for during device processing. Nevertheless, GaAs/AlGaAs sensors with resolution down to 100nm have been realised by electron beam lithography and wet etching

with very careful control of the process parameters [11]. The surface states of narrow gap semiconductors tend to lie in the conduction band and they do not typically suffer from sidewall depletion. It is relatively straightforward to pattern deep sub-micron GaSb/InAs/GaSb sensors, although care has to be taken to avoid a surface accumulation layer at exposed InAs surfaces. To date the smallest working Hall probes have been realised in Bi films, ironically the material that formed the basis of the very first Hall probe scanners over 40 years ago. Hall probes with spatial resolution of 50nm have been realised by milling a thin Bi film with a focussed ion beam [12]. These sensors do have rather poor NEFs, but were successfully used to map the stray fields at the surface of a Bi-substituted yttrium iron garnet film at 300K.

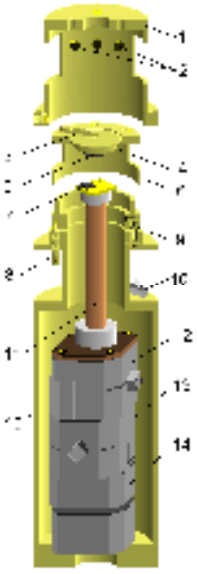

Fig. 2 (colour online) Sketch of a scanning Hall probe microscope head designed to fit on the cold flange of a commercial He-3 refrigerator. 1) receptacle tube, 2) LED array, 3) Bronze flat spring, 4) Sample holder disc, 5) Sample, 6) Sample holder cup, 7) Hall probe, 8) Alignment screw, 9) Extension bronze spring, 10) Electrical connectors, 11) Piezoscanner tube, 12),13) ANPx100 positioners, 14) ANPz100 positioner, 15) Brass microscope hull.

2.2. Sensor Geometry and Surface Tracking Modes

The spatial resolution of a scanning Hall sensor is fundamentally limited by the sample-sensor spacing. As a consequence sensor chips must be equipped with a secondary integrated sensor to map the sample topography and control the scan height. Frequently this takes the form of a scanning tunnelling microscopy (STM) tip micro-fabricated as close to the active Hall element as possible (c.f., Fig. 1(a))). Scanning *vector* Hall sensors have also been developed with STM-tracking based on MOVPE GaAs overgrowth of a micromachined GaAs pyramid [13]. Independent Hall probes patterned on three of the pyramidal faces allow the full magnetic field vector to be reconstructed.

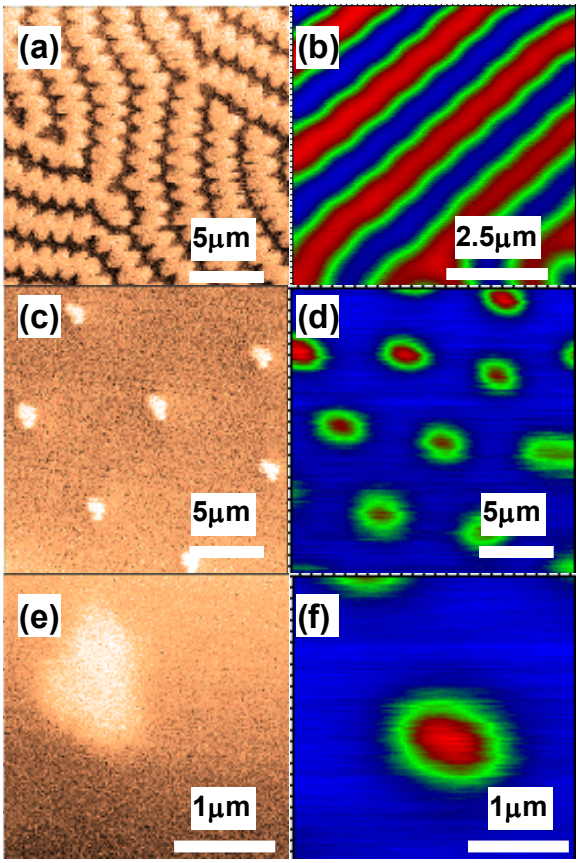

Fig. 3 (colour online) (a) MFM and (b) SHPM images of zig-zag distortions of domain walls in a YIG film at H=0. (c),(e) MFM and (d),(f) SHPM images of magnetic bubbles at H~1kOe.

STM tracking is very effective for well-connected conducting samples. However, in order to image insulating samples or isolated structures on insulating substrates, various sensors with atomic force tracking have been developed. Hall sensors have been integrated onto microfabricated cantilevers with additional piezoresistive force/deflection detection and a micromachined AFM tip (c.f. Fig. 1(b)) [14]. In a simpler approach it has become common to glue a Hall probe to a quartz crystal tuning fork force sensor [15]. In operation the force sensor assembly is dithered at its resonance frequency using a digital Phase Locked Loop, and frequency shifts used to map the topography in AFM tracking mode. There have also been a number of attempts to pattern Hall sensors directly on the end of AFM tips, although this has proved to be a very

challenging problem which has yet to be satisfactorily solved [16].

The final design criterion of a SHPM system is the choice of scanning and coarse approach mechanisms. Fig. 2 illustrates a SHPM head we have designed in Bath for mounting on the cold head of a commercial Oxford Instruments Heliox He-3 refrigerator [17]. This represents a rather common choice whereby linear "stick-slip" piezoelectric motors are used for coarse sensor positioning (labels 12, 13) and approach (label 14), while a four segment 2" long piezoelectric scanner tube (label 11) is employed for fine scanning.

3. Comparative MFM/SHPM Study of Labyrinth Domains in YIG Films

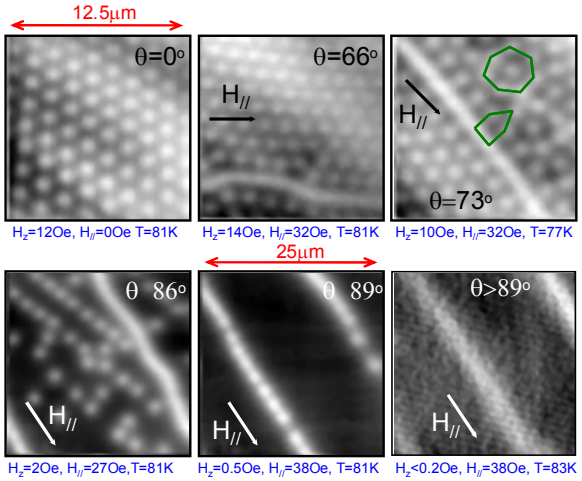

Fig. 4 (colour online) Set of SHPM images of crossing pancake and Josephson vortex lattices with the magnetic field applied at various indicated tilt angles away from the crystal c-axis.

It is crucial to understand the strengths and weaknesses of a given magnetic imaging approach and, in general, it is important to compare the results of two or more complementary techniques on the same magnetic sample. This is illustrated here in a comparative MFM/SHPM study of the structure of labyrinth domains in an Yttrium Iron Garnet film shown in Fig. 3. Figs. 3(a),(b) shows high resolution imaging of zig-zag wall distortions (which reduce the total magnetostatic field energy) at zero applied field. Evidently the zig-zag structure is much better resolved in the MFM images with a high coercivity tip, and only poorly seen in lower-resolution SHPM images. At the same time the more quantitative SHPM images show the expected equal 'up' and 'down' domain widths, while MFM maps exhibit pronounced asymmetry between attractive and repulsive magnetic forces. In an applied field of H~1kOe (Figs. 3(c)-(f)) the labyrinth domain structure breaks up into a lattice of magnetic bubbles. As before these bubbles are better resolved in MFM images, but the apparent 3-fold sub-structure is probably an image artefact due to tip-induced motion of the bubble and is never observed in the less invasive SHPM images.

4. Illustrative Examples of SHPM Imaging of Vortices

Figs. 4 and 5 illustrate some of the recent superconducting vortex imaging work we have performed with SHPM.

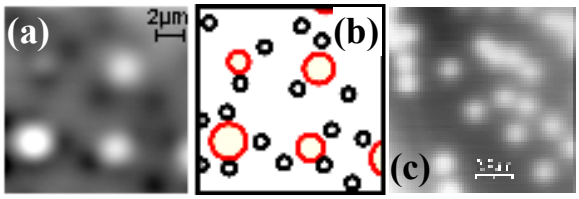

Fig. 5 (colour online) (a) SHPM image of vortex-antivortex molecules induced in a Pb film by the stray fields of an array of ferromagnetic dots. (b) Sketch of (a) highlighting positions of vortices above the magnetic dots (square array of large red circles) and antivortices outside the dots (small uniform diameter black circles) (c) SHPM image of vortices in a Sr_2RuO_4 single crystal at T=300mK in the earth's magnetic field.

Fig. 4 shows the results of an investigation of the role crystalline anisotropy plays in determining the nature of vortex matter. The very strong crystalline anisotropy in the high temperature cuprate superconductor $Bi_2Sr_2CaCu_2O_{8+\delta}$ (BSCCO) is reflected in the vortex (and vortex lattice) structure as a function of direction of applied field. Over a wide range of applied field angles tilted vortices are unstable with respect to forming "crossing" vortex lattices of orthogonal pancake and Josephson vortices. Furthermore these two sub-lattices weakly interact, leading to chains of pancake vortices where they have condensed out onto stacks of Josephson vortices at high tilt angles. This can be thought of as effectively representing the *Bitter decoration* of Josephson vortices by pancake vortices [18].

Fig. 5(a) shows an image of spontaneous vortex-antivortex 'molecules' generated by the stray fields of an array of ferromagnetic Co/Pt multilayer dots underneath a superconducting Pb film. Vortices (white) are trapped above the dot, while a shell of discrete antivortices (black) is induced in the superconductor just outside the dot by the returning stray fields [19].

Fig. 5(c) shows an image of vortices in the exotic superconductor Sr_2RuO_4, which is believed to be an odd-parity p-wave spin triplet (i.e., Cooper pairs have parallel spins) superconductor. Since the optimal T_c of this material is 1.5K this work has only recently been made possible by our development of an SHPM capable of operating below 300mK on a He-3 refrigerator [17]. In common with other groups that have performed magnetic imaging on this material [20] we see highly disordered vortex images with

pronounced spatial symmetry breaking (c.f., the stripe-like clustering running diagonally across the image). How these observations relate to the expected physics of this fascinating superconductor remains an open question.

5. Conclusions

The current state-of-the-art of scanning Hall probe microscopy has been described. The technique provides a valuable complement to other scanned probe magnetic imaging techniques; it is non-invasive, quantitative and can be used over a wide range of magnetic fields and temperatures. Considerable efforts are being devoted to the exploration of new Hall sensor materials for system optimisation under different experimental conditions, e.g. at room temperature and for high spatial resolution. Minimum detectable fields are still poor at 300K, but recent developments in narrow gap semiconductor quantum well technology promise to have a big impact in the area. The current state-of-the-art spatial resolution is 50nm in FIB-patterned Bi sensors. To significantly improve on this will require new ways of tracking the sensor across the sample, e.g., by perfecting techniques for fabricating a high performance Hall sensor on the end of an AFM tip.

6. Acknowledgments

This work was supported financially by EPSRC (GR/R46489/01, EP/D034264/1 & EP/E039944/1), the EU Marie Curie programme, the ESF VORTEX and NES networks, the Royal Society and the Leverhulme Trust.

References

[1] R.F.Broom and E.H.Rhoderick, Proc. Phys. Soc., **79**, 586 (1962).
[2] R.N.Goren and M.Tinkham, J. Low Temp. Phys. **5**, 465 (1971).
[3] H.W.Weber and R.Riegler, Sol. State Comm. **12**, 121 (1973).
[4] Y.Sugiyama and S.Kataoka, Proc. IEEE, **64**, 1643 (1976).
[5] R.Dingle, H.L.Stormer, A.C.Gossard and W.Wiegmann, Appl. Phys. Lett. **33**, 665 (1978).
[6] G.Binnig, H.Rohrer, C.Gerber and E.Weibel, Phys. Rev. Lett. **49**, 57 (1982).
[7] S.A.Solin, R.A.Stradling, T.Thio and J.W.Bennett, Meas. Sci. Technol. **8**, 1174 (1997).
[8] A.M.Chang, H.D.Hallem, L.Harriott, H.F.Hess, H.L.Kao, J.Kwo, R.E.Miller, R.Wolf, J.van der Ziel and T.Y.Chang, Appl. Phys. Lett. **61**, 1974 (1992).
[9] A.Oral, S.J.Bending and M.Henini, Appl. Phys. Lett. **69**, 1324 (1996).
[10] J.M.S.Orr, A.M.Gilbertson, M.Fearn, O.W.Croad, C.J.Storey, L.Buckle, M.T.Emeny, P.D.Buckle and T.Ashley, Phys. Rev. B **77**, 165334 (2008).
[11] J.S.Neal, H.G.Roberts, M.R.Connolly, S.Crampin, S.J.Bending, G.Wastlbauer and J.A.C.Bland, Utramicroscopy **106**, 614 (2006).
[12] A.Sandhu, K.Kurosawa, M.Dede and A.Oral, Jap. J. Appl. Phys. 1, **43**, 777 (2004).
[13] D.Gregusova, V.Cambel, J.Fedor, R.Kudela, J.Soltys, T.Lalinsky, I.Kostic and S.J.Bending, Appl. Phys. Lett. **82**, 3704 (2003).
[14] A.J.Brook, S.J.Bending, J.Pinto, A.Oral, D.Ritchie, H.Beere, M.Henini and A.Springthorpe, Appl. Phys. Lett. **82**, 3538 (2003).
[15] M.Dede *et al.*, J. Nanosci. Nanotechnol. **8**, 619 (2008).
[16] B.K.Chong, H.Zhou, G.Mills, L.Donaldson and J.M.R.Weaver, J. Vac. Sci. Technol. A **19**, 1769 (2001).
[17] V.V. Khotkevych, M.V. Milošević & S.J. Bending, Rev. Sci. Instr. **79**, 123708 (2008)
[18] A.N.Grigorenko *et al*., Nature **414**, 728 (2001).
[19] J.S.Neal *et al*., PRL 99, 127001 (2007).
[20] V. O Dolocan *et al*., Phys. Rev. Lett. **95**, 097004 (2005); Per G. Björnsson *et al*., Phys. Rev. B **72**, 012504 (2005)